Trop J Nat Prod Res, October 2025; 9(10): 4791 - 4797 **ISSN 2616-0684 (Print)**
ISSN 2616-0692 (Electronic)

Tropical Journal of Natural Product Research

Available online at https://www.tjnpr.org

Original Research Article

Zingiber officinale Extract Inhibits Entry of SARS-CoV-2 D614G Virus-Like Particles to 6HBE14o- cells: *In Vitro* and *In Silico* Approaches

Miftahul Mushlih[1,2], Marlita Marlita[3,4], Kavana H. Kusuma[1,5], Yuyun I. Christina[5,6], Dinia R. Dwijayanti[5,6,7], Dewi Mustikaningtyas[8], Nashi Widodo[5,6,7], Muhammad S. Djati[5,6,7]*, Sri Widyarti[7], Muhaimin Rifa'i[5,6,7]

[1]*Doctoral Program, Department of Biology, Faculty of Mathematics and Natural Sciences, Brawijaya University, Malang, East Java, Indonesia*
[2]*Faculty of Health Science, Universitas Muhammadiyah Sidoarjo, Sidoarjo, East Java, Indonesia*
[3]*Faculty of Mechatronics, Informatics and Interdisciplinary Studies, Technical University of Liberec, Liberec, Czech Republic*
[4]*Institute for Nanomaterials, Advanced Technologies and Innovation, Technical University of Liberec, Liberec, Czech Republic*
[5]*Dewan Jamu Indonesia East Java Region, Malang, East Java, Indonesia*
[6]*Innovation Center of Integrative Jamu and Eco-pharmaca, Brawijaya University, Malang 65145, East Java, Indonesia*
[7]*Department of Biology, Faculty of Mathematics and Natural Sciences, Brawijaya University, Malang, East Java, Indonesia*
[8]*Department of Biology, Faculty of Mathematics and Natural Sciences, Universitas Negeri Semarang, Semarang, Indonesia*

ARTICLE INFO

Article history:
Received 06 June 2025
Revised 15 September 2025
Accepted 19 September 2025
Published online 01 November 2025

ABSTRACT

Global public health systems are facing challenges due to the COVID-19 pandemic, which is caused by the Severe Acute Respiratory Syndrome Coronavirus 2 (SARS-CoV-2). Given increasing interest in plant-based antivirals, this study determined the potential of ethanol extract of red ginger (*Zingiber officinale*) to inhibit the attachment of SARS-CoV-2 virus-like particles (VLPs) to human bronchial epithelial cells. SARS-CoV-2 VLPs carrying the D614G spike mutation were generated in HEK293T cells using plasmids encoding the envelope (E), membrane (M), and spike-EGFP fusion proteins. EGFP was used to visualize and quantify VLP attachment. VLP formation was confirmed by fluorescence microscopy and transmission electron microscopy. Cells were exposed to 200 ng/mL of VLPs together with *Z. officinale* extract at 0.67 to 20 µg/mL for 24-48 h, and viral attachment was quantified via EGFP fluorescence intensity. For *in silico* analysis, identified compounds of *Z. officinale* extract were screened based on drug-likeness parameters for further processing to molecular docking and molecular dynamics simulations. The results showed that treatment with *Z. officinale* extract significantly reduced VLP attachment at concentrations of 0.67–10 µg/mL after 24 h. After 48 h, the lowest concentrations (0.67 and 1.25 µg/mL) maintained inhibitory effects from SARS-CoV-2 VLP, as indicated by reduced EGFP fluorescence. Of the 22 initially screened compounds, 9 met drug-likeness parameters. Among these, (2E)-3-(3,4-dimethoxyphenyl)prop-2-enoic acid and ferulic acid exhibited the strongest binding affinities to the SARS-CoV-2 spike protein (-5.3 and -5.5 kcal/mol, respectively). These findings suggest that *Z. officinale* contains bioactive compounds with potential as antiviral agents targeting SARS-CoV-2 variants.

Keywords: Antivirus, D614G Mutation**,** SARS-CoV-2, Virus-like particle, *Zingiber officinale*, *In silico*.

Introduction

Severe Acute Respiratory Syndrome Coronavirus 2 (SARS-CoV-2) has presented a previously unknown worldwide health threat since its appearance in early 2020.[1] SARS-CoV-2 is a positive-sense, enclosed, single-stranded RNA virus that belongs to the Coronaviridae family. Its diameter ranges from 60 to 140 nm.[2] The spike (S) glycoprotein, a crucial component of the virus, binds to the angiotensin-converting enzyme 2 (ACE2) receptor via its receptor-binding domain (RBD) to enable viral entry. ACE2 is highly expressed in multiple organs, including the lungs, heart, and kidneys, which contribute to the multisystemic manifestations of COVID-19.[3]

*Corresponding author. Email: msdjati@ub.ac.id
Tel: +62 813-3666-8909

Citation: Mushlih M, Marlita M, Kusuma KH, Christina YI, Dwijayanti DR, Mustikaningtyas D, Widodo N, Djati MS, Widyarti S, Rifa'i M. *Zingiber officinale* extract inhibits entry of SARS-CoV-2 D614G virus-like particles to 6HBE14o- cells: In vitro and in silico approaches. Trop J Nat Prod Res. 2025; 9(10): 4791 – 4797 https://doi.org/10.26538/tjnpr/v9i10.13

Official Journal of Natural Product Research Group, Faculty of Pharmacy, University of Benin, Benin City, Nigeria

Given the central role of the spike-ACE2 interaction in viral infection and pathogenesis, the spike protein remains a primary target for antiviral development. Although vaccination has reduced the severity and spread of COVID-19, the search for complementary antiviral agents remains essential. Natural products are gaining renewed attention due to their pharmacological properties, including antiviral activity.[4,5,6] Among these, red ginger (*Zingiber officinale* var. *rubrum*) has traditionally been utilized to enhance immune responses, particularly in respiratory infections, including COVID-19. *Z. officinale* is rich in bioactive constituents such as gingerol, shogaol, and paradol, which are associated with antimicrobial, anti-inflammatory, antioxidant, and anticancer effects.[7,8] Previous studies have demonstrated the antiviral effect of *Z. officinale* extracts against influenza (H1N1) and herpes simplex virus.[9,10] However, scientific evidence supporting its efficacy against SARS-CoV-2 remains limited, highlighting a critical research gap. Research on SARS-CoV-2 is often restricted by the need for high-containment laboratories (BSL-3/4).[11] Virus-like particles (VLPs), which structurally mimic the structure of native viruses but lack viral genomes, offer a safer alternative for evaluating viral entry and attachment under lower biosafety levels (BSL-1 or BSL-2).[12,13]Among the mutations identified in SARS-CoV-2, the D614G spike mutation has become one of the most prevalent mutations. It has been associated with increased viral infectivity and ACE2 binding efficiency.[14] D614G mutation enhances the stability of the spike protein and facilitates a

more open conformation of the receptor-binding domain, thereby promoting more efficient binding to the ACE2 receptor.[15] VLPs expressing D614G spike protein provide a practical model for preliminary screening of antiviral agents targeting viral attachment. Unlike previous research, this study specifically targets the D614G spike variant, one of the most infectious and widespread mutations, using a VLP-based system.

This study offers a novel approach by integrating *in vitro* and *in silico* methods to investigate the inhibitory potential of *Z. officinale* ethanol extract on the attachment of SARS-CoV-2 D614G VLPs to human bronchial epithelial cells. To the best of our knowledge, this is the first report demonstrating the potential of red ginger as an antiviral agent against SARS-CoV-2 using a VLP-based model. This research seeks to provide scientific evidence for the antiviral potential of red ginger and contribute to the development of plant-based therapeutics against SARS-CoV-2.

Materials and Methods

Plant collection and extraction

The rhizomes of red ginger (*Zingiber officinale* var. *rubrum*) were collected from the UPT Balai Materia Medika, Batu, East Java, Indonesia (7°52'03.7"S 112°31'11.1"E) in August 2022. The identification of the plant was performed by the same institution (specimen number 211229.JMH.L.R.003). The rhizomes of *Z. officinale* were cleaned, dried, and milled into fine powder.[16-17] The powdered rhizome was extracted with 96% ethanol with a ratio of sample-to-solvent of 1:10 (w/v) at room temperature for 72 h. The mixture was then filtered using filter paper, and the solvent was removed using a rotary evaporator (Buchi R-114, PT. BUCHI Indonesia) at 55°C to obtain the crude ethanol extract. The extract was stored at 4°C until further analysis.

SARS-CoV-2 VLP G614D Production

The SARS-CoV-2 G614D VLPs were generated using three plasmids encoding the envelope (E), membrane (M), and spike (S) proteins, with the spike protein fused to enhanced green fluorescent protein (EGFP) as a reporter. These plasmids were designed based on the GISAID database entry hCoV-19/Indonesia/EJ-ITD3590NT/2020 (EPI_ISL_437188, collected on 2020-04-14, Surabaya) and were cloned into the pcDNA3.1 expression vector. Plasmid synthesis was carried out by GenScript Biotech (Singapore). The plasmids were propagated and maintained in *Escherichia coli* and purified before use. The viability of *E. coli* cultures was ensured by their ability to grow in LB broth with the presence of ampicillin before plasmid extraction. Plasmid isolation was performed from actively growing bacterial cultures.

VLP production was performed in human embryonic kidney 293T (HEK-293T) cells, obtained from Elabscience® (Elabscience Biotechnology Inc., USA). The cells were cultured in Dulbecco's Modified Eagle Medium (DMEM; Gibco™, Thermo Fisher Scientific Inc., USA) supplemented with 10% fetal bovine serum (FBS; Gibco™, Thermo Fisher Scientific Inc., USA), 100 U/mL penicillin, and 100 µg/mL streptomycin. Cultures were maintained at 37°C in a humidified atmosphere containing 5% CO_2.

Transfection was initiated when the cells reached over 90% confluency, using an electroporation-based method.[18] Cells were harvested by trypsinization, centrifuged at 1500 rpm for 5 minutes at 4°C, and washed with 500 µL of ice-cold phosphate-buffered saline (PBS). Following homogenization and a second centrifugation, equal volumes (10 µL each) of the S-EGFP, M, and E plasmids were added to the cell suspension and gently mixed. The mixture was transferred to an electroporation cuvette and incubated on ice for 5 min. Electroporation was performed with five pulses at 1800 A, followed by a 10-minute recovery period on ice. The transfected cells were then transferred to a petri dish containing fresh culture medium. VLP-containing supernatants were harvested 48 h post-transfection.

For VLP isolation, the supernatant from transfected HEK-293T cells was collected and subjected to sequential centrifugation: first at 1000 rpm for 10 minutes at 4°C, then at 2000 rpm for an additional 10 minutes at 4°C to remove cell debris. The clarified supernatant was filtered and subsequently ultracentrifuged at 39,000 rpm for 4 hours through a 20% sucrose cushion. The resulting pellet was resuspended in PBS. The concentration of VLPs was determined using a NanoDrop spectrophotometer.

SARS-CoV-2 VLP G614D Characterization

The obtained VLPs were deposited onto carbon-coated grids for one minute, followed by a 45-second staining with UranyLess. Next, the samples were examined and photographed using a Transmission Electron Microscope (Hitachi HT-7700 TEM, Hitachi High-Technologies Corporation, Japan) at an operating voltage of 100 kV. For fluorescence analysis, HEK293T cells were cultured in a glass-bottom dish with complete medium. After 48 h, the EGFP expression was analyzed using the Bio-Imaging Navigator FSX100 Olympus at an excitation wavelength of 488 nm.

Determination of IC_{50} value of Z. officinale extract on 16HBE14o- cells

The IC_{50} value of *Z. officinale* extract on 16HBE14o- cells was assessed using the WST-1 method. Initially, 80,000 cells were seeded in a 96-well plate and incubated for 24 h in a controlled environment of 5% CO_2 at 37°C, using Alpha-MEM medium (Gibco™, Thermo Fisher Scientific, USA) enriched with 10% Fetal Bovine Serum (qualified Brazil, Gibco™, Thermo Fisher Scientific, USA), 2 mM L-glutamine solution (EmbryoMax®, Sigma-Aldrich, US) and 1% of 10,000 U/mL Penicillin/Streptomycin (Gibco™, Thermo Fisher Scientific, USA). Once the cells reached over 80% confluency, the medium was replaced with fresh medium containing various concentrations of the crude extract of *Z. officinale* (0, 21.875, 43.75, 87.5, 175, and 350 µg/mL) for 24 h. Then, the treatment medium was replaced and incubated with a complete medium containing 5% Cell Proliferation reagent WST-1 (Roche, Roche Diagnostics GmbH, Germany) for 30 min. The absorbance was recorded at 450 nm using a Microplate Reader (Model 680, Bio-Rad Laboratories, Inc., USA). The IC_{50} value was calculated through linear regression represented by the equation $Y=ax+b$. All experiment was performed in triplicate.

Inhibition assay of Z. officinale extract on VLP-SARS-CoV-2 G614D attachment

Cells were seeded at a density of 6×10^4 cells per well in 24-well plates with glass coverslips. Then, medium was replaced with a treatment medium containing *Z. officinale* extract (diluted 1/5 across concentrations ranging from 2.5 µM to 125 µM, with final DMSO concentration under 1%) and SARS-CoV-2 VLP (200 ng/ml). Before treatment, the mixture of VLP SARS-CoV-2 and *Z. officinale* extract was incubated at 37°C for 60 min. Observations were made after 24 and 48 h of treatment using a Confocal Laser Scanning Biological Microscope FV1000 Fluroview (Olympus®, Olympus Corporation, Japan). The experiments were performed in triplicate, and each culture was examined in four separate fields of view. To quantify the inhibition of viral attachment, the EGFP fluorescence area in infected cells was measured and compared to the reduced intensity of a control group without VLP SARS-CoV-2.

Bioactive compound profiling of Z. officinale rhizome extract

Approximately 5–10 mg of the *Z. officinale* extract was dissolved in 1 mL of methanol and transferred into a 1.5 mL vial. The mixture was subjected to sonication for 30 min to ensure complete dissolution, followed by filtration through a 0.22 µm polytetrafluoroethylene (PTFE) syringe filter. The filtered solution was subsequently analyzed using an ultra-high-performance liquid chromatography (UHPLC) system (Vanquish™ UHPLC Binary Pump, Thermo Scientific™, Germany) equipped with a Thermo Scientific™ Accucore™ Phenyl-Hexyl column (100 mm × 2.1 mm ID, 2.6 µm particle size). Chromatographic separation was achieved using a gradient elution with Mobile Phase A (0.1% formic acid in water, MS-grade) and Mobile Phase B (0.1% formic acid in acetonitrile, MS-grade) at a constant flow rate of 0.3 mL/min. The gradient started at 5% Mobile Phase B, increased linearly to 90% within 16 minutes, held for 4 minutes, and returned to the initial condition, resulting in a total run time of 25 minutes. The column temperature was maintained at 40°C, and the injection volume was 3 µL.

Detection of metabolites was carried out using the Q Exactive™ Hybrid Quadrupole-Orbitrap™ High-Resolution Mass Spectrometry (HRMS) system (Thermo Scientific™, Germany), operated in full MS and data-dependent MS2 (dd-MS2) acquisition modes under positive electrospray ionization (ESI). Nitrogen was used as the sheath gas (32 arbitrary units), auxiliary gas (8 arbitrary units), and sweep gas (4 arbitrary units). The ESI voltage was set at 3.30 kV, with the capillary temperature at 320°C and the auxiliary gas heater temperature at 30°C. The mass scanning range was set from m/z 66.7 to 1000, with a resolution of 70,000 for full MS and 17,500 for dd-MS2 mode. The acquired spectral data were processed using Compound Discoverer™ software version 3.2 (Thermo Fisher Scientific Inc., US). Background signals were subtracted by comparison with blank samples. Compound identification was performed via database matching using mzCloud™ (HighChem LLC, Slovakia) and ChemSpider™ (Royal Society of Chemistry, England), applying a mass accuracy tolerance of ±5 ppm. Identified compounds were selected based on a Z-Cloud similarity score greater than 80%, relative abundance, and confirmed presence in the PubChem database (https://pubchem.ncbi.nlm.nih.gov/).

Screening of bioactive compounds in Z. officinale rhizome extract

The biological activity of the compounds was further assessed using the PASS server (http://www.pharmexpert.ru/passonline), where the Pa value was used as an indicator of biological activity.[19] The analysis of potential drug compounds was conducted via SwissADME (https://www.swissadme.ch/), applying the Lipinski, Ghose, Veber, and Egan criteria. Compounds with no more than two violations of Lipinski's rule were retained for further evaluation.

Modeling of SARS-CoV-2 Spike Protein with D614G Mutation

The spike protein model of SARS-CoV-2 with the D614G mutation was sourced from the Swiss Model platform (https://swissmodel.expasy.org/interactive) by editing and aligning the target sequence with protein ID 6ZB5. Validation involved calculating the Root Mean Square Deviation (RMSD) through PyMOL (Schrodinger, USA), followed by assessments using ProQ scores (https://www.sbc.su.se) and a Ramachandran plot. The receptor-binding domain (RBD) was also selected and re-aligned with the RBD in protein 6ZB5.

Molecular docking analysis

AutoDock MGL Tools were used to assign Kollman charges, refine hydrogen bonding interactions, and add Gasteiger charges before the docking process. Ligands underwent energy minimization and were converted to the .pdbqt format using Open Babel, which was integrated into PyRx version 0.9.5 (PyRx, USA).[20] Molecular docking was conducted with AutoDock Vina version 1.1.2 (The Scripps Research Institute, USA) through PyRx 0.9.5, focusing on the receptor's binding site, specifically the active site of the RBD. The docking utilized a grid box with center coordinates of (-40.34, 30.85, 6.61) along the x, y, and z axes, and dimensions of 35 Å × 50 Å × 30 Å. The docked complexes were subsequently analyzed using the Protein.plus webserver (https://proteins.plus/).

Molecular dynamics simulation

Molecular dynamics (MD) simulations were conducted using YASARA (Yet Another Scientific Artificial Reality Application) version 23.4.25 (YASARA Biosciences GmbH, Austria) with the AMBER14 force field.[21] Ligand and receptor preparation followed the standard molecular docking protocol, ensuring consistency across simulation inputs. The simulation setup and execution utilized the md_run macro, while post-simulation analyses were performed using md_analyze and md_analyzeres macros. Key parameters assessed included root mean square deviation (RMSD) of the protein backbone and ligand, hydrogen bond interactions, and radius of gyration.

Simulations were performed on the ligand–RBD complexes exhibiting the highest binding affinity and fulfilling drug-likeness and antiviral selection criteria. In addition, curcumin (PubChem CID: 969516) was included as a reference control compound due to its well-documented antiviral.[22] All simulations were run under physiological conditions (temperature 37 °C, pH 7.4, pressure 1 atm) for a total duration of 50 nanoseconds. Trajectory analyses were used to evaluate the dynamic stability and interaction profiles of the ligand–RBD complexes, including the curcumin control.[23]

Data analysis

All data are expressed as the mean ± standard deviation (SD) from three independent experimental replicates. Before analysis, the raw data were normalized using the following formula:

$$\frac{(n-min.value)}{(max.value-min.value)}x100 \quad (1)$$

Quantification of EGFP fluorescence was conducted on a per-cell basis, with morphologically abnormal or syncytial cells excluded from the analysis. Statistical analyses were performed using IBM SPSS Statistics version 26 (IBM Corp., Armonk, NY). Group comparisons were conducted using the Kruskal–Wallis test, followed by Bonferroni post hoc correction. Differences were considered statistically significant at $p < 0.05$.

Results and Discussion

Production of SARS-CoV-2 D614G VLP and inhibitory potential of Z. officinale extract against SARS-CoV-2 VLP

The VLPs were produced using HEK293T cells, which expressed the structural proteins required for VLP formation, which subsequently underwent auto-assembly to form VLPs resembling SARS-CoV-2. After VLP formation, these particles were released into the culture medium. The medium was then harvested and purified through centrifugation. TEM revealed that the VLPs closely resembled the structure of the authentic SARS-CoV-2 virus, with visible spike proteins surrounding the particles (Figure 1). Measurement of the SARS-CoV-2 VLP size showed an average diameter of 90.33 ± 32.45 nm, consistent with the size of the original virus. The results showed the IC_{50} value of *Z. officinale* extract against 16HBE140-cells was 160 µg/mL. The IC_{50} value represents the concentration at which 50% of cell viability is inhibited, providing an estimate of the cytotoxicity level. This measurement is crucial in evaluating the safety and efficacy of *Z. officinale* extract, especially for potential therapeutic applications, where controlled inhibition of cellular activity or pathogenic mechanisms is desired. *In vitro* antiviral activity was performed using 16HBE14o- cells as the host. SARS-CoV-2 VLPs were mixed with ethanol extract of *Z. officinale* in the culture medium, and the VLP entry into the host cells was observed. *Z. officinale* extract exhibited antiviral effects, with varying levels of inhibition depending on the treatment time and concentration. After 24 h of treatment, a significant reduction in VLP entry into cells was observed at concentrations of 0.6, 1.25, 2.5, 5, and 10 ng/µL, indicating that the 24-h treatment was more effective at inhibiting VLP attachment and entry compared to the positive control. After 48-h treatment, a significant reduction occurred only at concentrations of 0.6 and 1.25 ng/µL, suggesting that prolonged incubation reduced the antiviral effectiveness at certain concentrations.

Identification of Z. officinale active compounds

The LC-HRMS analysis successfully identified 22 active compounds in the *Z. officinale* ethanol extract (Table 1). Then, all compounds were screened for drug-likeness based on Lipinski, Ghose, Veber, and Egan Rules. This analysis found that 9 compounds passed drug-likeness screening, including D-(+)-Pipecolinic acid, pyridoxine, (-)-caryophyllene oxide, 6-gingerol, octhilinone (OIT), 6-shogaol, (+)-ar-turmerone, ferulic acid, (2E)-3-(3,4-dimethoxyphenyl) prop-2-enoic acid, and *α*-linolenic acid meet Lipinski, Ghose, Veber, and Egan drug-likeness criteria (Figure 2A). None of the identified compounds exhibited significant antiviral activity against coronaviruses (Figure 2B). On the other hand, other viruses, such as Rhinovirus and Picornavirus, which are RNA viruses from the Picornaviridae family, demonstrated significant antiviral activity with almost all identified active compounds. Additionally, the active compounds showed antiviral potential against Influenza (family Orthomyxoviridae) and HIV (family Retroviridae). Overall, *α*-Linolenic acid exhibited the highest antiviral potential compared to other compounds, followed by

ISSN 2616-0684 (Print)
ISSN 2616-0692 (Electronic)

(2E)-3-(3,4-dimethoxyphenyl) prop-2-enoic acid.

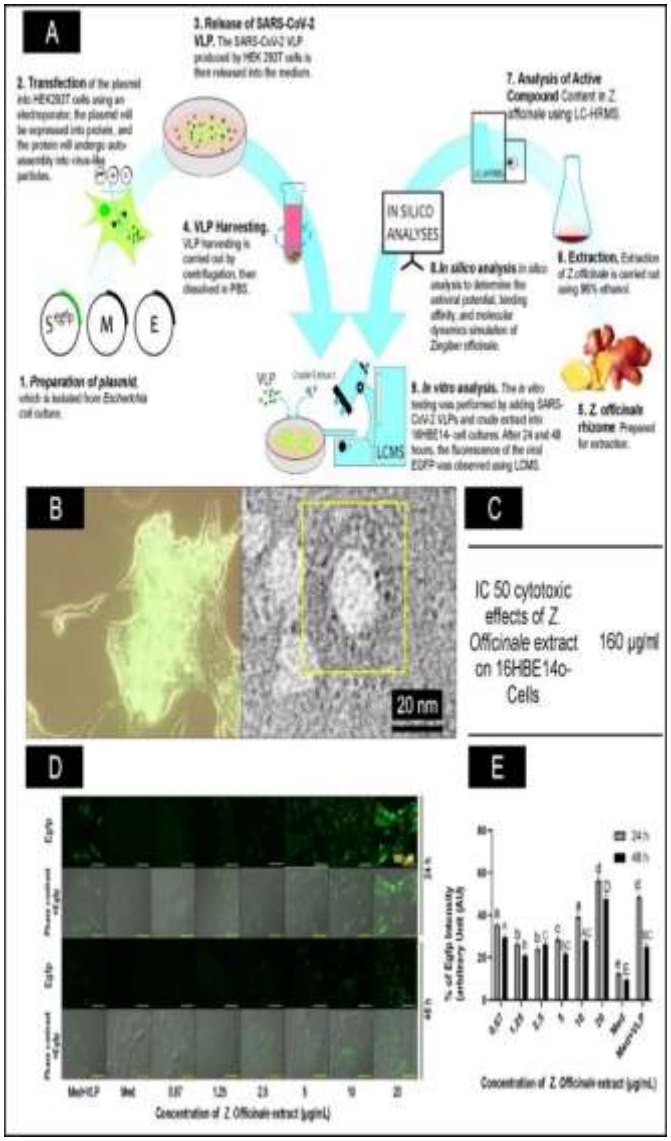

Figure 1: The characterization and production of SARS-CoV-2 VLP and the analysis of the inhibitory potential of *Z. officinale* extract in blocking the attachment of SARS-CoV-2 VLP to host cells. (A) The research workflow scheme: (B) HEK293T cells producing SARS-CoV-2 VLP, with green fluorescence indicating the presence of EGFP on the VLP; (C) TEM image where the structure of the SARS-CoV-2 VLP is visible, surrounded by Spike proteins (yellow box); (D) The inhibitory effect of *Z. officinale* extract using CLMS; (E) EGFP fluorescence intensity analysis. The different subset indicates a significantly lower fluorescence level compared to the positive control after 24 h of treatment (p-value < 0.05), while the ^ indicates a significantly lower fluorescence after 48 h of treatment (p-value < 0.05).

Molecular docking and dynamic simulation results

Receptor Binding Domain (RBD) modeling of SARS-CoV-2 (RBD-SARS-CoV-2) was conducted to introduce the D614G mutation, and the model was validated (Figure 2B). The identified active compounds were then docked with the RBD. The binding affinity analysis between the active compounds and SARS-CoV-2 D614G RBD showed the lowest values for (+)-ar-turmerone (-6.2 kcal/mol), ferulic acid (-5.5 kcal/mol), (-)-caryophyllene oxide (-5.5 kcal/mol), D-(+)-pipecolinic acid (-5.4 kcal/mol), (2E)-3-(3,4-dimethoxyphenyl) prop-2-enoic acid (-5.3 kcal/mol), 6-shogaol and 6-gingerol (-5.2 kcal/mol), *α*-linolenic acid (-5 kcal/mol), pyridoxine (-4.9 kcal/mol), and octhilinone (OIT) (-4.5 kcal/mol).

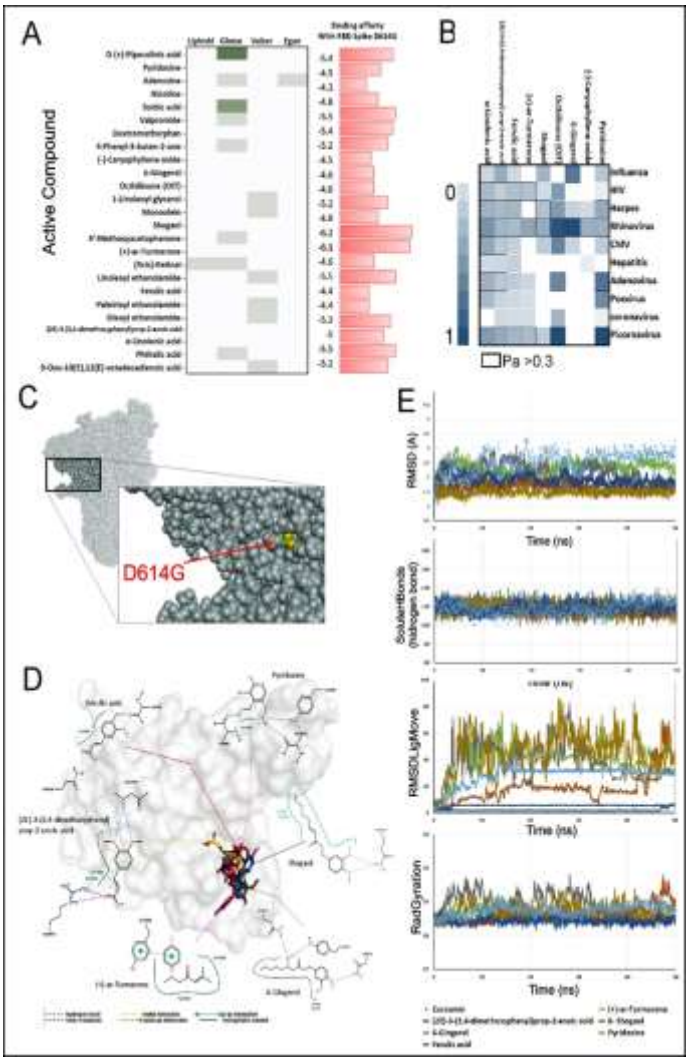

Figure 2: *In silico* analysis and the potential of *Z. officinale* extract in inhibiting the attachment of SARS-CoV-2 VLP to host cells. (A) Drug-likeness analysis using Lipinski, Ghose, Veber, and Egan rules; (B) Spike protein modeling of SARS-CoV-2 with the D614G mutation; (C) Antiviral potential analysis of active compounds from *Z. officinale*; (D) Biological activity of active components from *Z. officinale* in inhibiting the entry of SARS-CoV-2 VLP; (E) Molecular dynamic simulation with RMSD bd, RMSD ligMove (nm), Sollute H bind, & RadGyration.

Antiviral potential analysis indicated that *α*-linolenic acid possesses the most significant antiviral activity compared to other compounds, particularly against rhinovirus and picornavirus. Other active compounds with high potential include 6-gingerol, pyridoxine, and octhilinone (OIT). The remaining active compounds also exhibit antiviral potential, although at lower levels. Further analysis was conducted using MD simulations, focusing on compounds with strong binding interactions identified in the protein binding analysis. This analysis revealed six active molecules that had been previously selected. In the Root Mean Square Deviation for the Binding Domain (RMSDbd) analysis, all six compounds demonstrated stability up to 50

ns.

Table 1: Analysis of active compounds in *Z. officinale* using LC-HRMS

Name	Formula	RT [min]	CID	References
D-(+)-Pipecolinic acid	$C_6H_{11}NO_2$	0.825	7405	Chen *et al*.[24]
Pyridoxine	$C_8H_{11}NO_3$	1.121	1054	Sari and Nasuha[25]
Sorbic acid	$C_6H_8O_2$	3.506	643460	Ezez and Tefera[8] Zhang *et al*.[15]
Valpromide	$C_8H_{17}NO$	8.268	71113	-
4-Phenyl-3-buten-2-one	$C_{10}H_{10}O$	9.528	637759	Kuo *et al*.[26]
(-)-Caryophyllene oxide	$C_{15}H_{24}O$	9.853	1742210	Suherman and Maulidya[27]
6-Gingerol	$C_{17}H_{26}O_4$	10.417	442793	Suherman and Maulidya[27]
Octhilinone (OIT)	$C_{11}H_{19}NOS$	10.958	33528	-
1-Linoleoyl glycerol	$C_{21}H_{38}O_4$	11.604	5283469	Rao *et al*.[28]
Monoolein	$C_{21}H_{40}O_4$	12.08	5283468	Katerina *et al*.[29]
6- Shogaol	$C_{17}H_{24}O_3$	12.231	5281794	Suherman and Maulidya[27]
4'-Methoxyacetophenone	$C_9H_{10}O_2$	13.103	7476	Nakazawa and Ohsawa[30]
(+)-ar-Turmerone	$C_{15}H_{20}O$	13.127	160512	Račková *et al*.[31]
(9cis)-Retinal	$C_{20}H_{28}O$	13.573	6436082	Sari and Nasuha[25]
Linoleoyl ethanolamide	$C_{20}H_{37}NO_2$	13.677	5283446	-
Ferulic acid	$C_{10}H_{10}O_4$	13.791	445858	Liu *et al*.[32] Zhang *et al*.[15]
Palmitoyl ethanolamide	$C_{18}H_{37}NO_2$	13.863	4671	Nievergelt *et al*.[33]
Oleoyl ethanolamide	$C_{20}H_{39}NO_2$	14.307	5283454	Arias-Gaguancela and Chapman[34]
(2E)-3-(3,4-dimethoxyphenyl)prop-2-enoic acid	$C_{11}H_{12}O_4$	14.631	717531	Ahmad *et al*.[35]
α-Linolenic acid	$C_{18}H_{30}O_2$	14.668	18402199 2	Liu *et al*.[32]
Phthalic acid	$C_8H_6O_4$	17.648	1017	Račková *et al*.[31]
9-Oxo-10(E),12(E)-octadecadienoic acid	$C_{18}H_{30}O_3$	17.843	5283011	Saraç *et al*.[36]

The RMSD Ligand Movement (RMSD lig move) analysis indicated that ferulic acid and (2E)-3-(3,4-dimethoxyphenyl) prop-2-enoic acid exhibited high stability, while 6-shogaol showed high stability but began to change between 42-50 ns. 6-gingerol displayed instability initially but stabilized after 33 ns, maintaining stability until the end. The other compounds (pyridoxine and (+)-ar-turmerone) showed instability. The analysis of the number of hydrogen bonds and radius of gyration indicated stability across all analyzed compounds.

SARS-CoV-2 VLPs were successfully constructed using three key plasmids encoding the spike (S), envelope (E), and membrane (M) proteins. The S plasmid was engineered with an enhanced green fluorescent protein (EGFP) tag to enable visualization of VLP formation.[37] Fluorescence microscopy confirmed the expression of EGFP, while TEM revealed spherical particles surrounded by crown-like formations, which are characteristic features of SARS-CoV-2. The average diameter of the resulting VLPs was 52.94 ± 27.32 nm, smaller than previously reported diameters (129 ± 32 nm),[37] possibly due to differences in structural protein expression systems or the host cell line used for production.[38] These findings confirm successful generation of SARS-CoV-2 VLPs that mimic key morphological features of the native virus.

The cytotoxicity assay revealed an IC_{50} value of *Z. officinale* extract was 160 µg/mL, indicating moderate cytotoxicity. This indicates that concentrations below this IC_{50} value could be safely used in antiviral applications. Notably, *Z. officinale* extract demonstrated antiviral activity at all tested concentrations. Significant reductions in VLP entry were observed at 0.67 and 1.25 µg/mL after 48 h of treatment, and at concentrations ranging from 0.67–10 µg/mL after 24 h. This suggests that *Z. officinale* extract effectively blocks viral attachment, particularly during shorter exposure durations. The enhanced antiviral effect at 24 h compared to 48 h may reflect the instability or degradation of active compounds over time. Interestingly, at higher concentrations of *Z. officinale* extract (20 µg/mL), the virus entered the cells in greater numbers. This may be due to non-specific effects of the extract on cell membrane integrity or receptor expression, which could facilitate viral uptake. These results highlight the need for careful optimization of *Z. officinale* extract's concentrations in future applications.

Further evaluation through molecular docking between active compounds and the Spike D614G model showed that (+)-ar-Turmerone exhibited the lowest binding affinity (-6.2 kcal/mol), followed by ferulic acid (-5.5 kcal/mol). The next lowest binding affinities were found in (-)-Caryophyllene oxide and (2E)-3-(3,4-dimethoxyphenyl)prop-2-enoic acid. To further assess the stability of these active compounds, a molecular dynamics (MD) simulation was conducted. The RMSD lig-mov analysis indicated that ferulic acid and (2E)-3-(3,4-dimethoxyphenyl)prop-2-enoic acid exhibited the most stable binding, with RMSD_lig-mov values of 5.4 Å and 1.9 Å, respectively (Figure 2E). Other compounds, including (+)-ar-Turmerone, 6-Shogaol, 6-Gingerol, and pyridoxine, showed much higher RMSD_lig-mov values (>18 Å), indicating poor stability within the binding site and potential ligand drift.[39] On the other hand, the analysis of the number of hydrogen bonds and radius of gyration showed stable values. The instability observed in the RMSD ligand movement suggests that the ligand does not remain fixed within the binding site. Although key interactions (H-bonds) are maintained, other parts of the ligand may move freely or shift, indicating that the overall ligand-protein binding might be weak or suboptimal.

The findings suggest that (2E)-3-(3,4-dimethoxyphenyl) prop-2-enoic acid is a promising candidate for further development as a SARS-CoV-2 entry inhibitor. The reduced efficacy observed at 48 h may reflect degradation or reduced bioavailability of active compounds within *Z. officinale* extract. Further purification and formulation studies are needed to enhance the stability and delivery of these bioactive constituents. Despite its contributions, this study is constrained by the exclusive use of the D614G spike variant, while many other SARS-CoV-2 variants have since evolved. Moreover, the lack of *in vivo* experimentation limits the assessment of pharmacokinetics and systemic safety. Future research should incorporate animal models and clinical investigations to establish therapeutic relevance.

Conclusion

This study confirms that SARS-CoV-2 D614G VLPs were successfully produced through fluorescence and electron microscopy methods. The ethanol extract of *Z. officinale* demonstrated significant efficacy in inhibiting SARS-CoV-2 VLP attachment to 16HBE14o- cells at low concentrations, although higher concentrations resulted in increased viral penetration. *α*-linolenic acid and (2E)-3-(3,4-dimethoxyphenyl)prop-2-enoic acid showed the strongest antiviral potential, supported by stable molecular interactions in simulation studies. These findings highlight *Z. officinale* as a promising source of antiviral agents against SARS-CoV-2.

Conflict of Interest

The authors declare no conflict of interest.

Authors' Declaration

The authors hereby declare that the work presented in this article is original and that any liability for claims relating to the content of this article will be borne by them.

Acknowledgements

The authors would like to express their gratitude to the National Research and Innovation Agency (BRIN) and the Indonesia Endowment Funds for Education (LPDP) for their financial support in this research through the Research and Innovation Funding Program for Advanced Indonesia (grant number 32/IV/KS/06/2022 and 1612.1/UN10.C10/TU/2022).

References

1. Lai CC, Shih TP, Ko WC, Tang HJ, Hsueh PR. Severe acute respiratory syndrome coronavirus 2 (SARS-CoV-2) and coronavirus disease-2019 (COVID-19): The epidemic and the challenges. Int J Antimicrob Agents. 2020;55(3):1-9. doi: 10.1016/j.ijantimicag.2020.105924.
2. Zu ZY, Jiang MD, Xu PP, Chen W, Ni QQ, Lu GM, Zhang LJ. Coronavirus Disease 2019 (COVID-19): A perspective from China. Radiology. 2020;296(2):E15-E25. doi: 10.1148/radiol.2020200490.
3. Wang YT, Landeras-Bueno S, Hsieh LE, Terada Y, Kim K, Ley K, Shresta S, Saphire EO, Regla-Nava JA. Spiking pandemic potential: structural and immunological aspects of SARS-CoV-2. Trends Microbiol. 2020;28(8):605-618. doi: 10.1016/j.tim.2020.05.012.
4. Erharuyi O, Aghahowa S, Igbinosa E, Imieje VO, Ogbeide OK, Akhigbe IU, Nahandoo I, Olowoeyo BE, Akubuiro PC, Ayorinde J, Igoli JO, Falodun A. Anti-SARS-CoV-2 activity and acute toxicity screening of *Annona muricata* and *Artemisia annua* Leaf Extracts. Trop J Nat Prod Res. 2024;8(1):6028-6034. doi: 10.26538/tjnpr/v8i1.45.
5. Rizma BRP, Ananto AD, Sunarwidhi AL. The study of potential antiviral compounds from Indonesian medicinal plants as anti-COVID-19 with molecular docking approach. J Mol Docking. 2021;1(1):32–39. doi: 10.33084/jmd.v1i1.2307.
6. Zhan Y, Ta W, Tang W, Hua R, Wang J, Wang C, Lu W. Potential antiviral activity of isorhamnetin against SARS-CoV-2 spike pseudotyped virus in vitro. Drug Dev Res. 2021;82(8):1124-1130. doi: 10.1002/ddr.21815.
7. Dahham SS, Tabana YM, Iqbal MA, Ahamed MB, Ezzat MO, Majid AS, Majid AM. The anticancer, antioxidant and antimicrobial properties of the sesquiterpene β-caryophyllene from the essential oil of *Aquilaria crassna*. Molecules. 2015;20(7):11808-11829. doi: 10.3390/molecules200711808.
8. Ezez D, Tefera M. Effects of solvents on total phenolic content and antioxidant activity of ginger extracts. J Chem. 2021;2021(1):1-5. doi: 10.1155/2021/6635199.
9. Nur'aini AL, Hartati S, Untari T. In ovo inhibition of avian pox virus replication by mangosteen rind and red ginger ethanolic extracts. Vet World. 2021;14(10):2640-2645. doi: 10.14202/vetworld.2021.2640-2645.
10. Untari T, Widyarini S, Wibowo MH. Antiviral activity of the essential oil of red ginger on Avian Influenza. Vet. J. 2013;13(3):309–312.
11. Mignaqui AC, Ferella A, Cass B, Mukankurayija L, L'Abbé D, Bisson L, Sánchez C, Scian R, Cardillo SB, Durocher Y, Wigdorovitz A. Foot-and-Mouth Disease: Optimization, Reproducibility, and Scalability of High-Yield Production of Virus-Like Particles for a Next-Generation Vaccine. Front Vet Sci. 2020;7:1-9. doi: 10.3389/fvets.2020.00601.
12. Gourdelier M, Swain J, Arone C, Mouttou A, Bracquemond D, Merida P, Saffarian S, Lyonnais S, Favard C, Muriaux D. Optimized production and fluorescent labeling of SARS-CoV-2 virus-like particles. Sci Rep. 2022;12(1):1–15. doi: 10.1038/s41598-022-18681-z.
13. Le DT, Müller KM. In vitro assembly of virus-like particles and their applications. Life. 2021;11(4):1-18. doi: 10.3390/life11040334.
14. Korber B, Fischer WM, Gnanankaran S, Yoon H, Theiler J, Abfalterer W, Foley B, Giorgi EE, Bhattacharya T, Parker M, Partridge D, Evans C, de Silva TI, on behalf of the Sheffield COVID-19 Genomics Group, LaBranche CC, Montefiori DC. Spike mutation pipeline reveals the emergence of a more transmissible form of SARS-CoV-2. BioRxiv. 2020; 1–33. doi: 10.1016/j.cell.2020.06.043
15. Zhang S, Kou X, Zhao H, Mak KK, Balijepalli MK, Pichika MR. *Zingiber officinale* var. rubrum: red ginger's medicinal uses. Molecules. 2022;27(3):1-31. doi: 10.3390/molecules27030775.
16. Djati MS, Christina YI, Rifa'i M. The combination of *Elephantopus scaber* and *Sauropus androgynus* promotes erythroid lineages and modulates follicle-stimulating hormone and luteinizing hormone levels in pregnant mice infected with Escherichia coli. Vet World. 2021;14(5):1398-1404. doi: 10.14202/vetworld.2021.1398-1404.
17. Christina YI, Rifa'i M, Widodo N, Djati MS. Comparative study of antiproliferative activity in different plant parts of *Phaleria macrocarpa* and the underlying mechanism of action. Sci World J. 2022;2022:1-13. doi: 10.1155/2022/3992660.
18. Rohmah IN, Marlita M, Kusuma KH, Christina YI, Dwijayanti DR, Mustikaningtyas D, Widodo N, Djati MS. Corrigendum: Evaluating SARS-CoV-2 spike protein transfection in HEK-293T cells for VLP applications. J Exp Life Sci. 2025;15(2):45-51. doi: 10.21776/ub.jels.2025.015.02.01.
19. Christina YI, Nafisah W, Atho'illah MF, Rifa'i M, Widodo N, Djati MS. Anti-breast cancer potential activity of *Phaleria macrocarpa* (Scheff.) Boerl. leaf extract through in silico studies. J Pharm Pharmacogn Res. 2021;9(6):824–845. doi: 10.56499/jppres21.1092_9.6.824
20. Masruri M, Safitri A, Ulfa SM, Ferdian RF, Fabri ARA, Karta IW, Harrist M, Shalsadila AA. Phytochemical composition, antioxidant activity, and metabolite profiling of sequential extracts from *Vitex trifolia* leaves with Antibacterial potential: An integrated *in vitro* and *in silico* study. Trop J Nat Prod Res. 2025; 9(7):291-2991. doi: 10.26538/tjnpr/v9i7.5
21. Krieger E, Vriend G. New ways to boost molecular dynamics simulations. J Comput Chem. 2015;36(13):996-1007. doi: 10.1002/jcc.23899.
22. Suravajhala R, Parashar A, Choudhir G, Kumar A, Malik B, Nagaraj VA, Padmanaban G, Polavarapu R, Suravajhala P, Kishor PBK. Molecular docking and dynamics studies of curcumin with COVID-19 proteins. Netw Model Anal Health Inform Bioinform. 2021;10(1):1-44. doi: 10.1007/s13721-021-00312-8.
23. Deeba F, Malik MZ, Naqvi IH, Haider MSH, Shafat Z, Sinha P, Ishrat R, Ahmed A, Parveen S. Potential entry inhibitors of the envelope protein (E2) of Chikungunya virus: in silico

structural modeling, docking and molecular dynamic studies. Virusdisease. 2017;28(1):39-49. doi: 10.1007/s13337-016-0356-2.
components shogaols in mouse and human urine and modulation of the glutathione levels in cancer cells by [6]-shogaol. Mol Nutr Food Res. 2013;57(3):447-458. doi: 10.1002/mnfr.201200679.
25. Sari D, Nasuha A. Nutrients content, phytochemical, and pharmacological activities of ginger (*Zingiber officinale* Rosc.): A review. Trop Biosci J Biol Sci 2021;1(2):11–18. doi: 10.32678/tropicalbiosci.v1i2.5246.
26. Kuo PC, Damu AG, Cherng CY, Jeng JF, Teng CM, Lee EJ, Wu TS. Isolation of a natural antioxidant, dehydrozingerone from *Zingiber officinale* and synthesis of its analogues for recognition of effective antioxidant and antityrosinase agents. Arch Pharm Res. 2005;28(5):518-528. doi: 10.1007/BF02977752.
27. Suherman M, Maulidya SAI. In silico study: secondary metabolites from red ginger rhizome (*Zingiber officinale* var. Rubrum) as potential inhibitors OF3CLpro and PLpro of SARS-CoV-2. Med Sains. 2023;8(3):1249–1262. doi: 10.37874/ms.v8i3.810.
28. Rao MJ, Tahir Ul Qamar M, Wang D, Ali Q, Ma L, Han S, Duan M, Hu L, Wang L. A high-throughput lipidomics and transcriptomic approach reveals novel compounds from sugarcane linked with promising therapeutic potential against COVID-19. Front Nutr. 2022;9:1-15. doi: 10.3389/fnut.2022.988249.
29. Katerina V, Klara U, Samnang N, Ladislav K. Chemical Composition of Essential Oils and Supercritical Carbon Dioxide Extracts from *Amomum kravanh*, *Citrus hystrix* and *Piper nigrum* 'Kampot'. Molecules. 2023;28(23):1-16. doi: 10.3390/molecules28237748.
30. Nakazawa T, Ohsawa K. Metabolism of [6]-gingerol in rats. Life Sci. 2002;70(18):2165-2175. doi: 10.1016/s0024-3205(01)01551-x.
31. Račková L, Cupáková M, Tažký A, Mičová J, Kolek E, Košt'álová D. Redox properties of ginger extracts: Perspectives of use of *Zingiber officinale* Rosc. as antidiabetic agent. Interdiscip Toxicol. 2013;6(1):26-33. doi: 10.2478/intox-2013-0005.
24. Chen H, Soroka DN, Hu Y, Chen X, Sang S. Characterization of thiol-conjugated metabolites of ginger
32. Liu H, Yang H, Zhao T, Lin C, Li Y, Zhang X, Ye Y, Liao J. Combined metabolome and transcriptome analyses of young, mature, and old rhizome tissues of *Zingiber officinale* Roscoe. Front Genet. 2021;12:1-16. doi: 10.3389/fgene.2021.795201.
33. Nievergelt A, Marazzi J, Schoop R, Altmann KH, Gertsch J. Ginger phenylpropanoids inhibit IL-1beta and prostanoid secretion and disrupt arachidonate-phospholipid remodeling by targeting phospholipases A2. J Immunol. 2011;187(8):4140-4150. doi: 10.4049/jimmunol.1100880.
34. Arias-Gaguancela O, Chapman KD. The biosynthesis and roles of n-acylethanolamines in plants. Adv Bot Res. 2022;101:345–373. doi: 10.1016/bs.abr.2021.07.002.
35. Ahmad B, Rehman MU, Amin I, Arif A, Rasool S, Bhat SA, Afzal I, Hussain I, Bilal S, Mir Mu. A Review on pharmacological properties of zzingerone (4-(4-Hydroxy-3-methoxyphenyl)-2-butanone). Sci World J. 2015;2015:1-6. doi: 10.1155/2015/816364.
36. Saraç H, Demirbaş A, Tüzün B. Could *Zingiber officinale* plant be effective against omicron BA.2.75 of SARS-CoV-2?. Turk Comput Theor Chem. 2023;7(3):42–56. Doi: 10.33435/tcandtc.1198612
37. Swann H, Sharma A, Preece B, Peterson A, Eldredge C, Belnap DM, Vershinin M, Saffarian S. Author Correction: Minimal system for assembly of SARS-CoV-2 virus like particles. Sci Rep. 2021;11(1):9352. doi: 10.1038/s41598-021-88846-9.
38. Xu R, Shi M, Li J, Song P, Li N. Construction of SARS-CoV-2 Virus-Like Particles by mammalian expression system. Front Bioeng Biotechnol. 2020;8:1-6. doi: 10.3389/fbioe.2020.00862.
39. Halder SK, Sultana I, Shuvo MN, Shil A, Himel MK, Hasan MA, Shawan MMAK. In silico identification and analysis of potentially bioactive antiviral phytochemicals against SARS-CoV-2: A molecular docking and dynamics simulation approach. Biomed Res Int. 2023;2023:1-32. doi: 10.1155/2023/5469258.